Clinical decision support tool for the identification of pathological structures associated with age-related macular degeneration

Iván Barrientos[1,2], Joaquim de Moura[1,2*], Jorge Novo[1,2], Marcos Ortega[1,2], and Manuel G. Penedo[1,2]
{ivan.barrientos.lema, joaquim.demoura, jnovo, mortega, mgpenedo}@udc.es

[1] Grupo VARPA, Instituto de Investigación Biomédica de A Coruña (INIBIC), Universidade da Coruña, A Coruña, (Spain)
[2] Centro de investigación CITIC, Universidade da Coruña, A Coruña, (Spain)

Abstract. In the field of ophthalmology, different imaging modalities are commonly used to carry out different clinical diagnostic procedures. Currently, both optical coherence tomography (OCT) and optical coherence tomography angiography (OCT-A) have made great advances in the study of the posterior pole of the eye and are essential for the diagnosis and monitoring of the treatment of different ocular and systemic diseases. On the other hand, the development of clinical decision support systems is an emerging field, in which clinical and technological advances are allowing clinical specialists to diagnose various pathologies with greater precision, which translates into more appropriate treatment and, consequently, an improvement in the quality of life of patients. This paper presents a clinical decision support tool for the identification of different pathological structures associated with age-related macular degeneration using OCT and OCT-A images. The system provides a useful tool that facilitates clinical decision-making in the diagnosis and treatment of this relevant disease.

Keywords: CAD system, Deep learning, OCT, OCT-A, AMD

1 Introduction

Age-related macular degeneration (AMD) represents one of the leading causes of vision loss in older adults. This relevant eye disease is an age-related condition that results from a gradual deterioration of light-sensitive cells in the tissue at the back of the eye. Specifically, AMD mainly affects peripheral blood vessels, causing different signs of systemic and retinal vascular deterioration. New emerging ophthalmic imaging technologies, such as optical coherence tomography (OCT) and optical coherence tomography angiography (OCT-A), have great potential to support early diagnosis of this relevant eye disease. On the one hand, OCT is a non-invasive imaging technique that uses low-coherence light to capture two-dimensional and three-dimensional micro-resolution scans of the

retina, allowing a more precise evaluation of its main morphological structures. On the other hand, OCT-A is a more recent technique for the capture of high-resolution images of the choroidal and retinal circulations without the need for dye injections. In particular, OCT-A detects the blood movement using intrinsic signals to capture the precise location of the blood vessels. Consequently, this ophthalmological test has great potential to improve the understanding of the pathophysiology of the eye fundus, providing relevant information for the diagnosis and monitoring of the AMD treatment.

Given the great relevance of this topic, several authors have addressed the development of intelligent systems for the identification, segmentation and characterisation of different regions of clinical interest using OCT and OCT-A images. As reference, in the field of OCT imaging, we can find different proposals for the precise identification of different morphological structures, such as retinal layers [6, 5] or retinal vessels [11, 10]. We can also find different proposals for the segmentation of regions with the presence of pathological fluid or the presence of the epiretinal membrane [2, 1]. On the other hand, in the field of OCT-A imaging, different methodologies have been proposed for the identification of structures of clinical interest [9, 3] or the calculation of different computational biomarkers [12, 4]. Despite the considerable efforts that were made to develop automated methods to support clinical diagnosis, there is still no platform that integrates OCT and OCT-A images for the diagnosis of AMD, so this problem is only partially addressed.

Taking this into account, in this work, we present a clinical decision support tool for the identification of different pathological structures associated with AMD using OCT and OCT-A, two widely used imaging modalities with great diagnostic potential. For this purpose, we have designed a fully automatic solution based on deep learning strategies, which is initially composed of three complementary modules. A first module that automatically distinguishes between OCT and OCT-A images; it is useful to differentiate the type of image for a more accurate and efficient diagnosis. The second module is able to differentiate healthy patients from those with the following pathologies on OCT images: choroidal neovascularization (CNV), diabetic macular edema (DME) and drusen. The third module is able to automatically classify the OCT-A images as retinal vein occlusion (RVO) or healthy. Finally, these modules were integrated into a web platform, offering different functionalities, such as patient management or the intuitive visualisation of results through clinical reports, facilitating the work of ophthalmologists.

2 Materials and methods

2.1 Dataset

OCT dataset. This dataset consists of 84,484 OCT images, corresponding to 26,315 healthy patients, 37,205 patients diagnosed with CNV, 11,348 patients diagnosed with DME and 8,616 patients with the presence of drusen deposits. Therefore, this dataset contains 4 classes (NORMAL, CNV, DME and

DRUSEN). All OCT images were selected from retrospective cohorts of adult patients from the Shiley Eye Institute at the University of California San Diego, the California Retinal Research Foundation, Medical Center Ophthalmology Associates, and the Beijing Tongren Eye Center. This dataset is publicly available to the scientific community [8].

OCT-A dataset. This dataset consists of 1,551 images obtained by an OCT-A capture device (Topcon DRI OCT Triton Plus swept source), where 870 are images of patients diagnosed with RVO and 681 are images without the presence of RVO. Therefore, two classes (RVO and NON-RVO) are analysed in this work. Specifically, these images were obtained at the Complejo Hospitalario Universitario de Santiago (CHUS) from different patients in accordance with the Declaration of Helsinki.

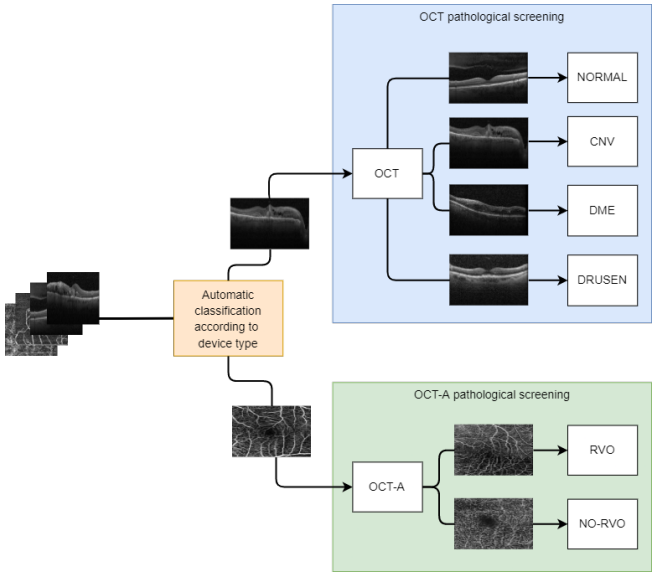

Fig. 1: Schematic representation of 3 computational modules to support the diagnosis of different ocular diseases.

2.2 Methodology

Figure 1 shows a schematic representation of the different computational modules that were developed for pathological screening. Each of these modules is explained in more detail below.

Module of classification according to device type. For the design of a clinical decision support tool based on the integration of different smart modules,

it is very useful to differentiate the type of image we are working with. As a consequence, we can obtain more accurate, reliable and repeatable results. With this in mind, we have designed a fully automatic module for image classification between OCT and OCT-A classes.

Module of OCT pathological screening. This smart module is able to differentiate automatically healthy patients from those diagnosed with the pathologies present in the OCT dataset. Specifically, OCT images will be classified into CNV for patients with choroidal neovascularisation, DME for patients with diabetic macular edema, DRUSEN for patients with presence of drusen deposits and NORMAL for healthy patients.

Module of OCT-A pathological screening. In this smart module, the system is able to automatically classify the OCT-A images between patients diagnosed with retinal vein occlusion (RVO) or healthy patients (NON-RVO).

2.3 Training details

In this work, we exploit the potential of the DenseNet-161 [7] architecture pretrained on the ImageNet dataset. For the training process, we have divided the datasets into mutually exclusive subsets for training (60%), validation (20%) and testing (20%). In addition, a cross-entropy loss function was used to adjust the weights of the models during the training stage. Regarding the optimisation of the model, Stochastic Gradient Descent was used with a learning ratio constant of 0.01, a mini-batch size of 16 and a first order momentum of 0.9. Finally, in order to achieve consistent results, the training step was repeated 5 times with random samples, which allows to calculate the averages of the results obtained and thus to evaluate the overall performance of all the proposed smart modules.

2.4 Clinical Decision Support Tool

All the smart modules, developed in this work, were integrated into a clinical decision support tool, facilitating clinical decision making in the diagnosis and treatment of AMD using OCT and OCT-A images. In addition, this web-based platform offers different functionalities, such as patient management or the intuitive visualization of results through different clinical reports that can be exported to PDF format or sent automatically by e-mail. This tool is fully scalable, allowing easy integration of new smart modules to support the diagnosis of new diseases or other types of medical imaging.

3 Results and Discussion

In this section, we present the experimental results of the proposed computational modules for the automatic identification of different pathological structures related to AMD using OCT and OCT-A images. For the validation of each

smart module, the following metrics are calculated: Accuracy, Precision, Recall and F1-score.

1^{st} Analysis: Classification according to device type. In this first analysis, we studied the performance of the proposed system to classify the input images according to 2 types of devices: (OCT and OCT-A). As expected, the system was able to adequately classify all images contained in the analyzed dataset, since it is a simple classification problem. In this sense, the obtained results demonstrate the powerful learning capability of deep neural networks to extract discriminative features for medical image analysis.

2^{nd} Analysis: OCT pathological screening. In this second analysis, we studied the performance of the proposed system to classify OCT images according to 4 classes: (NORMAL, CNV, DME and DRUSEN). Figure 2a shows the progression of the accuracy and Figure 2b the progression of the loss, both for the training and for the validation stages, considering 5 independent repetitions. As we can see, the training process has been completed after model stabilization before 40 epochs, obtaining accuracy values close to 1 for training and 0.975 for validation.

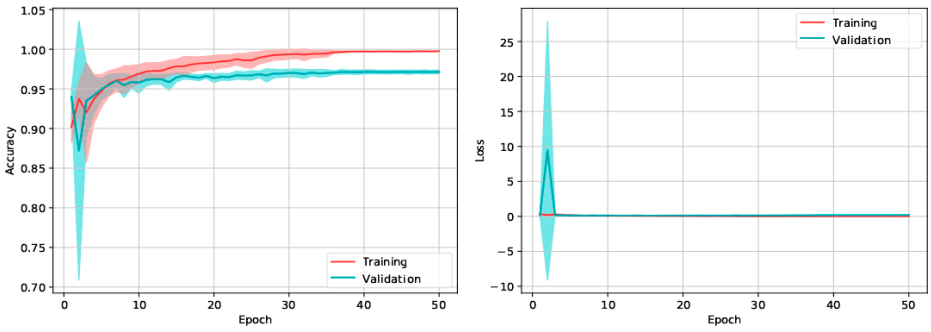

(a) (b)

Fig. 2: Results of the second analysis after 5 independent repetitions, in terms of mean ± standard deviation. (a) Representation of the evolution of accuracy in training and validation. (b) Representation of the evolution of loss in training and validation.

Complementarily, Table 1 shows the performance measures obtained in the test stage. As we can see, satisfactory results were obtained for each category, reaching a mean accuracy value of 0.9718 ± 0.0011. In particular, we can observe that the highest value obtained for the F-score is 0,9826 ± 0,0018 for the NORMAL class. On the contrary, the lowest value obtained for the F-score is 0,9103 ± 0,0041 for the DRUSEN class.

Class	*Recall*	*Precision*	*F1-score*
NORMAL	0,9838 ± 0,0013	0,9814 ± 0,0037	0,9826 ± 0,0018
CNV	0,9807 ± 0,0020	0,9808 ± 0,0024	0,9808 ± 0,0019
DME	0,9598 ± 0,0059	0,9680 ± 0,0029	0,9639 ± 0,0034
DRUSEN	0,9122 ± 0,0059	0,9085 ± 0,0069	0,9103 ± 0,0041

Table 1: Recall, Precision and F1-score for each class of the module of OCT pathological screening using the test dataset.

3^{rd} Analysis: OCT-A pathological screening. In this third analysis, we studied the performance of the proposed system to classify OCT-A images according to 4 classes: (RVO and NON-RVO). Once again, Figure 2a illustrates the progression of the accuracy, as well as Figure 2b the progression of the loss, for both training and validation stages, considering 5 independent repetitions. As we can see, in this case, the training process has been completed after the stabilization of the model before 75 epochs, both for training and validation stages. As for the loss, we can see a very large variation in the initial epochs, but as accuracy stabilises, the loss decreases considerably, reaching values close to 0.

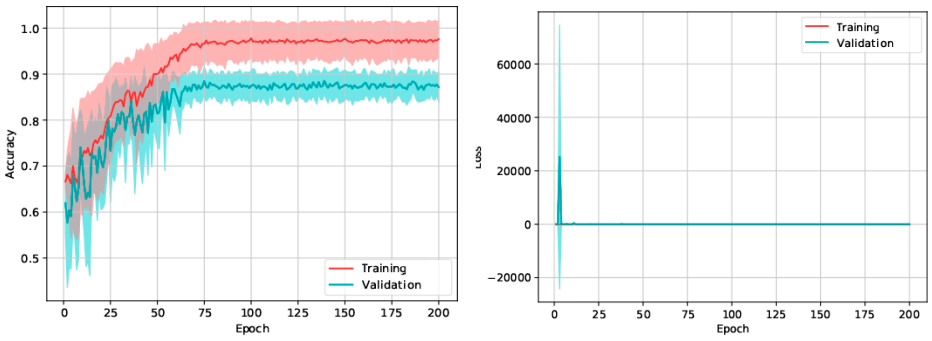

(a) (b)

Fig. 3: Results of the third analysis after 5 independent repetitions, in terms of mean ± standard deviation. (a) Representation of the evolution of accuracy in training and validation. (b) Representation of the evolution of loss in training and validation.

Additionally, we present the Table 2 with the values obtained for each class and represented by the Recall, Precision and F1-score metrics. In general, the results that were obtained by the proposed system with the test dataset are satisfactory, since it achieves a mean accuracy value of 0.8695 ± 0.0414. As we can see, the obtained results demonstrate the suitability of the model for the identification of different pathological structures related to AMD using OCT-A imaging.

Class	*Recall*	*Precision*	*F1-score*
RVO	0,8757 ± 0,0239	0,8890 ± 0,0519	0,8823 ± 0,0360
NON-RVO	0,8615 ± 0,0681	0,8455 ± 0,0323	0,8534 ± 0,0486

Table 2: Recall, Precision and F1-score for each class of the module of OCT-A pathological screening using the test dataset.

4 Conclusions

In this work, we propose a clinical decision support tool for the identification of different pathological structures associated with AMD using OCT and OCT-A images. For this purpose, we have designed a fully automatic solution based on deep learning, which is initially composed of 3 smart modules. A first module that automatically distinguishes between OCT and OCT-A images. The second module is able to differentiate healthy patients from those with the following pathologies on OCT images: CNV, DME and drusen deposits. The third module is able to automatically classify the OCT-A images as RVO or healthy patients. Finally, these modules were integrated into a web platform, offering different functionalities, such as patient management or the intuitive visualisation of results through clinical reports, facilitating the work of the ophthalmologists. Two representative datasets have been used for the validation of this work. The first dataset is composed of 84,484 OCT images differentiated into four classes: (NORMAL, CNV, DME and DRUSEN). The second dataset is composed of 1,551 OCTA images differentiated into two classes: (RVO and NON-RVO). The proposed system provided accurate results in all the designed smart modules, demonstrating a significative potential in the early diagnosis, treatment and monitoring of AMD.

Acknowledgements

This research was funded by Instituto de Salud Carlos III, Government of Spain, DTS18/00136 and PI17/00940 research projects; Ministerio de Ciencia e Innovación y Universidades, Government of Spain, RTI2018-095894-B-I00 research project; Ministerio de Ciencia e Innovación, Government of Spain through the research project with reference PID2019-108435RB-I00; Consellería de Cultura, Educación e Universidade, Xunta de Galicia, Grupos de Referencia Competitiva, grant ref. ED431C 2020/24 and postdoctoral grant ref. ED481B 2021/059; Axencia Galega de Innovación (GAIN), Xunta de Galicia, grant ref. IN845D 2020/38; CITIC, Centro de Investigación de Galicia ref. ED431G 2019/01, receives financial support from Consellería de Educación, Universidade e Formación Profesional, Xunta de Galicia, through the ERDF (80%) and Secretaría Xeral de Universidades (20%).

References

1. Sergio Baamonde, Joaquim de Moura, Jorge Novo, José Rouco, and Marcos Ortega. Feature definition and selection for epiretinal membrane characterization in optical coherence tomography images. In *International Conference on Image Analysis and Processing*, pages 456–466. Springer, 2017.

2. Joaquim de Moura, Plácido L Vidal, Jorge Novo, José Rouco, and Marcos Ortega. Feature definition, analysis and selection for cystoid region characterization in Optical Coherence Tomography. *Procedia computer science*, 112:1369–1377, 2017.
3. Macarena Díaz, Joaquim de Moura, Jorge Novo, and Marcos Ortega. Automatic wide field registration and mosaicking of OCTA images using vascularity information. *Procedia Computer Science*, 159:505–513, 2019.
4. Macarena Díaz, Jorge Novo, Paula Cutrín, Francisco Gómez-Ulla, Manuel G Penedo, and Marcos Ortega. Automatic segmentation of the foveal avascular zone in ophthalmological OCT-A images. *PLoS One*, 14(2):e0212364, 2019.
5. Leyuan Fang, David Cunefare, Chong Wang, Robyn H Guymer, Shutao Li, and Sina Farsiu. Automatic segmentation of nine retinal layer boundaries in OCT images of non-exudative AMD patients using deep learning and graph search. *Biomedical Optics Express*, 8(5):2732–2744, 2017.
6. A González-López, J de Moura, J Novo, M Ortega, and MG Penedo. Robust segmentation of retinal layers in optical coherence tomography images based on a multistage active contour model. *Heliyon*, 5(2):e01271, 2019.
7. Gao Huang, Zhuang Liu, Laurens Van Der Maaten, and Kilian Q Weinberger. Densely connected convolutional networks. In *Proceedings of the IEEE conference on computer vision and pattern recognition*, pages 4700–4708, 2017.
8. Daniel S Kermany, Michael Goldbaum, Wenjia Cai, Carolina CS Valentim, Huiying Liang, Sally L Baxter, Alex McKeown, Ge Yang, Xiaokang Wu, Fangbing Yan, et al. Identifying medical diagnoses and treatable diseases by image-based deep learning. *Cell*, 172(5):1122–1131, 2018.
9. Rachel Linderman, Alexander E Salmon, Margaret Strampe, Madia Russillo, Jamil Khan, and Joseph Carroll. Assessing the accuracy of foveal avascular zone measurements using optical coherence tomography angiography: segmentation and scaling. *Translational vision science & technology*, 6(3):16–16, 2017.
10. Joaquim de Moura, Jorge Novo, José Rouco, Manuel G Penedo, and Marcos Ortega. Automatic detection of blood vessels in retinal OCT images. In *International Work-Conference on the Interplay Between Natural and Artificial Computation*, pages 3–10. Springer, 2017.
11. Meindert Niemeijer, Mona K Garvin, Bram van Ginneken, Milan Sonka, and Michael D Abramoff. Vessel segmentation in 3D spectral OCT scans of the retina. In *Medical Imaging 2008: Image Processing*, volume 6914, pages 597–604. SPIE, 2008.
12. Harpal Singh Sandhu, Mohammed Elmogy, Ahmed Taher Sharafeldeen, Mohamed Elsharkawy, Nabila El-Adawy, Ahmed Eltanboly, Ahmed Shalaby, Robert Keynton, and Ayman El-Baz. Automated diagnosis of diabetic retinopathy using clinical biomarkers, optical coherence tomography, and optical coherence tomography angiography. *American journal of ophthalmology*, 216:201–206, 2020.